Author Manuscript

Published in final edited form as:

Med Eng Phys. 2017 Jun;44:87-93.

Doi: 10.1016/j.medengphy.2017.02.013

Title:

Comparative assessment of intrinsic mechanical stimuli on knee cartilage and compressed agarose constructs

A. Completo[1], C. Bandeiras[1], F. Fonseca[2]

[1] Mechanical Engineering Department, University of Aveiro, Portugal

[2] Orthopedics Department, Coimbra University Hospital, Portugal

ABSTRACT

A well-established cue for improving the properties of tissue-engineered cartilage is mechanical stimulation. However, the explicit ranges of mechanical stimuli that correspond to favourable metabolic outcomes are elusive. Usually, these outcomes have only been associated with the applied strain and frequency, an oversimplification that can hide the fundamental relationship between the intrinsic mechanical stimuli and the metabolic outcomes. This highlights two important key issues: the firstly is related to the evaluation of the intrinsic mechanical stimuli of native cartilage; the second, assuming that the intrinsic mechanical stimuli will be important, deals with the ability to replicate them on the tissue-engineered constructs. This study quantifies and compares the volume of cartilage and agarose subjected to a given magnitude range of each intrinsic mechanical stimulus, through a numerical simulation of a patient-specific knee model coupled with experimental data of contact during the stance phase of gait, and agarose constructs under direct-dynamic compression. The results suggest that direct compression loading needs to be parameterized with time-dependence during the initial culture period in order to better reproduce each one of the intrinsic mechanical stimuli developed in the patient-specific cartilage. A loading regime which combines time periods of low compressive strain (5%) and frequency (0.5Hz), in order to approach the maximal principal strain and fluid velocity stimulus of the patient-specific cartilage, with time periods of high compressive strain (20%) and frequency (3Hz), in order to approach the pore pressure values, may be advantageous relatively to a single loading regime throughout the full culture period.

***KeyWords*:** finite element models, tibiofemoral contact, pore pressure, maximal principal strain, fluid velocity, tissue-engineering.

1. INTRODUCTION

A general drawback of the regenerative concepts for degenerated and traumatic joints is that newly formed tissue lacks the structural organization of articular cartilage (AC) and has inferior mechanical properties [1-3]. A well-established cue for improving the mechanical properties of tissue-engineered cartilage is mechanical stimulation [4-9]. Of all mechanical loading regimes, direct dynamic compression is the most reported loading regime on chondrocyte seeded agarose constructs [10-15]. In spite of these efforts, it has been proven to be very difficult to achieve tissue-engineered cartilage outcomes that match native cartilage properties [3, 16]. Moreover, these outcomes depend largely on the loading parameters used [11, 17-18]. Usually these outcomes have only been related with true strain and applied frequency [11-14], an oversimplification that can hide the fundamental relationship between mechanical stimulation and the metabolic/mechanical outputs. Some authors [18-19] have found relationships between the intrinsic mechanical stimuli developed in cartilage explants and chondrocyte-seeded agarose constructs and the metabolic outcomes synthesis. From these studies, two important key issues in tissue-engineered cartilage arise: the first is related to the evaluation of the intrinsic mechanical stimuli of native cartilage in-vivo; the second, assuming that the intrinsic mechanical stimuli will be important, deals with the ability to replicate these stimuli on the agarose constructs. Therefore, our aim in this study was to quantify the volume fraction of cartilage and agarose subjected to a given magnitude range of each intrinsic mechanical stimulus, through a numerical simulation of a patient-specific knee model coupled with experimental data of contact knee biomechanics during the stance phase of gait [20] and agarose constructs under direct-dynamic compression, in order to identify the loading regime that better reproduces each one of the intrinsic mechanical stimulus developed in the patient-specific cartilage model.

2. MATERIALS AND METHODS

2.1 Numerical model of specific-patient knee associated with experimental gait data

One healthy subject aged 52 years with a body mass index of 24.5 Kg/m^2 without history of knee joint pathologies was used for the development of a specimen-specific knee finite element model. This model was developed with the aid of computed tomography (CT) and magnetic resonance (MR) scans of the patient's knee. Femoral and tibial bone models were generated from CT with scanning parameters as follows: 120 kVP, 330mAs, matrix size of 512x512 and pixel size of 0.488mm x 0.488mm. The slice thickness values were 0,5 mm. The mean total slices of the CT scan images were 1857 slices. During CT scanning, a calibration phantom was placed under the leg in order to enable future calculation of the bone mineral density. This CT scans were used to reconstruct the bone elements using ScanIP software (ScanIP, Simpleware Ltd., Exeter, UK). To get the bone elements mask, was utilized the thresholding method for CT bone elements. The Hounsfield (HU) scale range of the default CT bone thresholding was between 226 and 3071. The bone structures were meshed semi-automatically using four-noded tetrahedral elements (ScanFE, Simpleware Ltd., Exeter, UK), with the mapped specimen-specific bone material properties from CT (0.5mm slices thickness) data. The average number of elements were 64825 and 52687 in the femur and tibia, respectively (Figure 1). The linear relationship between apparent density (ρ) and HU was taken from the literature [21]. The power law for Young's Modulus (E), $E=1.990\rho^{3.46}$, proposed by Keller [22] was applied in this analysis. The cartilage was modelled using biphasic theory, as a solid phase with permeability, with a Newtonian fluid whose flow is governed by Darcy's law. The cartilage layers were reconstructed from the MR using a fast spoiled gradient echo sequence with the following imaging parameters: TR=26.7ms, TE=6.7ms, flip angle=20°, slice thickness=1.5 mm, matrix size=512x512, in-plane resolution=0.27 mm. Afterwards, the MR-imaging cartilage was segmented using ScanIP. Then the 3D geometry of the knee joint was constructed. Surface geometry of the knee cartilage was further imported into CATIA (Catia, Dassault-Systèms, France) where was transformed into a solid geometry. This was then imported into the FE modelling package Abaqus v. 6.10 (Simulia, Providence, RI) in which the FE mesh was created from 59514 8-node brick elements (C3D8RP).

Four layers of elements between the articulating and bony sides at the contact region were considered in order to take into account the variation of the elastic modulus of the solid matrix along the cartilage depth [23]. The equivalent Young's modulus for the Neo-Hookean solid matrix was set to 0.26 MPa, 0.38MPa, 0.5MPa and 0.5Mpa at the first, second, third and fourth layers respectively, with a Poisson's ratio of 0.15 in the first layer and 0.26 for the three others [23]. It is well known that hydraulic permeability of AC is deformation dependent [24]. Empirical exponential equations for the deformation-dependent permeability of cartilage have been shown to be accurate over a wide range of permeabilities [24-25]. van der Voet [26] proposed a formulation of an exponential law for deformation-dependent permeability that can be implemented in Abaqus:

$$k = k\_0\ ((e - e\_0)/(1 + e\_0\ ))\text{^}M \quad (1)$$

in which k_0 is the initial permeability, M is a positive constant, and e and e_0 are the current and initial void ratios, respectively. We used the values proposed by Wilson et al. [27] for the constants: M = 5, k_0 = 1.5 x 10^{-15}m4/Ns and e_0 = 3. The mass continuity of the fluid was satisfied using the pore fluid volumetric flux of each element. The fluid viscosity is constant and assumed to be equal to the viscosity of water at 37ºC, that is, 0.62 $g.m^{-1}s^{-1}$. Frictionless contact was considered between femoral and tibial cartilages. The nonlinear surface to surface contact discretization based on the hard contact constraint was chosen and a linear penalty method was used for the contact constraint enforcement.

The loading patterns applied to the specimen-specific tibiofemoral model were taken from in-vivo experimental data during the stance phase of gait [20], which were measured in 10% intervals of stance phase, evaluating contact location, contact area, thickness at contact area and resultant magnitude of cartilage contact deformation. Peak femur displacement was determined by multiplying peak tibiofemoral contact deformation data at 0%, 30%, 60% and 90% of stance phase by the specimen-specific cartilage thickness at the contact region, in order to achieve the nearest cartilage deformation value of the experimental data at the medial and lateral compartments (Table 1). The

cyclic displacement was imposed on the femur relatively to the fixed tibia at 1Hz, during 60 seconds. Each load cycle was computed with 100 time increments.

2.2 Numerical model of chondrocyte-seeded agarose constructs

Agarose constructs were modelled as cylinders with 8 mm diameter and 6 mm thickness. The numerical model was constituted by the upper compression plate, the agarose construct and the lower compression plate. The compression plates were considered impermeable, deformable and in frictionless contact with the agarose construct. The compression plates were made of polyethylene with a Young´s modulus of 2.1 GPa and a Poisson ratio of 0.3, and meshed with 1536 linear elastic brick elements. The agarose constructs also had a biphasic mechanical formulation. The construct was meshed with 12580 8-node brick elements, trilinear displacement, trilinear pore pressure and reduced integration (C3D8RP) using Abaqus v. 6.10 (Simulia, Providence, RI). The mechanical properties for the linear elastic solid phase were based on data for agarose 3% (w/v) hydrogels [28-32]. A Young's modulus of 133 kPa and a Poisson's ratio of 0.3 were considered [19]. The properties defined for the fluid phase and porous behavior were the initial permeability (k_0), specific weight of the wetting fluid (γ) and the initial void ratio (e_0). Permeability was defined as deformation-dependent using the following exponential law [33].

$$k = k\_0 * \exp(M * (e - e\_0)/(1 + e\_0)) \quad (2)$$

We used the following values M = 4.1 [30], $k_0 = 5 \times 10^{-12}$m4/N.s, $e_0 = 4$ [19] and $\gamma = 9731$N.m^{-3}[34]. The top and bottom surfaces of the agarose construct were free to move during upper plate compression movement. Briefly, fluid inflow and outflow from the lateral surface of construct were free, which was modelled with a zero pore pressure boundary condition. Nine direct dynamic compression cyclically loading regimes at the physiological level were simulated. These nine load regimes applied were the result of a combination of three true strain magnitudes of 5%, 10% and 20% with three applied frequencies of 0.5Hz, 1Hz and 3Hz. To achieve a steady state regime with a

reasonable computation time the nine loading regimes were applied for 60s, and each load cycle was computed with 100 time increments.

The intrinsic mechanical stimuli analysed in the specimen-specific tibiofemoral model and agarose constructs model were: pore fluid pressure, maximum principal strain and relative fluid velocity. The pore-pressure presumably stimulates cells to synthesise proteoglycans (PGs), the function of which is to resist pressure [33], while maximum principal strain/stress presumably is a stimulus for cells to generate collagen fibers [35], whose function is to resist tension. Finally, the relative fluid velocity can be related with glycosaminoglycan (GAG) synthesis [18]. For consistency of the comparison between the tibiofemoral cartilage and agarose construct models, the mechanical outcomes were compared when the mechanical response reached stability (steady state) during the last loading cycle. Each intrinsic mechanical stimulus was averaged at the integration point of each element at each time increment during the last load cycle. To quantify and compare the volume of cartilage and agarose subjected to a given magnitude range of each intrinsic mechanical stimulus during the last full load cycle, the volume fraction (in percentage) of cartilage and agarose was calculated according to the following equations:

$$V(t) = \{V_{el}(\bar{x}, t)\}, \qquad \bar{x} \in [x_{min}, x_{max}]$$

$$\phi = \left(\int_{t_i}^{t_f} \left(\sum_{i=1}^{m} \frac{V_i(t)}{V_0} \right) dt \right) * 100, \qquad t_i = t_f - T, \qquad T = \frac{1}{f} \tag{3}$$

where ϕ refers to the volume fraction, t_i and t_f the initial and the end times of the last compression cycle, V_o the indeformable volume of cartilage or agarose construct, m the number of elements of cartilage or agarose construct in volume V_o and V_i(t) the element volume for the intrinsic mechanical parameter $\bar{x}$ in the magnitude range between x_{min} and x_{max}. In the case of tibiofemoral cartilage the volume V_o was defined by the volume of cartilage delimited by the maximum contact area at each period (0%, 30%, 60% and 90%) of stance phase. This procedure was repeated for all loading regimes with a script written in MATLAB v. 7.0 (The Mathworks Inc., MA, USA).

3. RESULTS

The peak contact pressures on the articular surfaces of the patient-specific model were 0.2 MPa, 1.9 MPa, 0.5MPa, and 0.9Mpa at 0%, 30%, 60%, and 90% of stance phase respectively, which are in agreement with previously reported data [35-36]. It is noteworthy that arbitrary variations of the cartilage model parameters by ± 10% of the quoted values did not significantly alter the characteristics profiles of the three intrinsic mechanical stimuli analysed.

Figure 2 presents the volume fractions of agarose and cartilage in a given maximal principal strain range. For a compressive strain until 10% combined with all applied frequencies most of the agarose volume presented a maximal principal strain value below 0.03 m/m. At the cartilage model, most of the volume delimited by the contact area is below a maximal principal strain of 0.03m/m, with cartilage fraction volumes between 84.6% and 94.1%.

In Figure 3 the volume fraction of agarose and cartilage in a given pore-pressure range is depicted. For compressive strains until 10%, combined with all applied frequencies, most of the agarose volume (58.8% to 89.5%) has a pore pressure below 0.0035MPa. In the cartilage, most of the volume delimited by the contact area is above 0.0035Mpa, with a maximum of 80.9% of volume at 30% of the stance phase. All periods of stance phase analysed presented values of pore pressure greater than 0.021MPa (the maximum found at the agarose construct) with 4.2%, 47.9%, 26.7% and 25.5% of cartilage volume at 0%, 30%, 60%, and 90% of stance phase respectively.

Figure 4 presents the volume fraction of agarose and cartilage in a given fluid velocity range. For the compressive strains up to 10% and for all applied frequencies, most of the agarose volume 54.1% to 60.9% was between $1x10^{-6}$m/s and $13x10^{-6}$m/s. In the cartilage, most of the volume delimited by the contact area is below a fluid velocity of $0.165x10^{-6}$m/s, with a maximum of 94.2% and a minimum of 83.3% of volume at 0% and 30% of stance phase respectively.

4. DISCUSSION

Previous *in-vivo* studies have demonstrated the alignment of collagen fibers along the tensile principal strain direction [31]. Accordingly, maximum principal strain may be an intrinsic mechanical stimulus for cells to generate collagen fibres in the direction of these strains [38]. In our study, most of the cartilage volume during the stance phase was exposed to maximal principal strains lower than 0.03m/m. In a general way, the agarose construct model presented tensile principal strain values in the range of the cartilage model for the nine applied regimes. However, the agarose volume fraction on a given maximal principal strain range was very different among the applied loading regimes. For the 10% strain at 1Hz, one of the most common applied loading regimes in tissue-engineering constructs [10-14], the volume of agarose exposed to tensile principal strain greater than 0.03m/m was 45.8%, while the maximum for the cartilage model was of 15.4%. Of all loading regimes applied on the agarose model, the one that resembles the most the volume fraction of the given strain range on the cartilage was the loading regime of 5% of compression for all applied frequencies. Moreover, the agarose construct models showed more homogeneous tensile principal strain fields than the cartilage, where highly inhomogeneous strain fields were observed.

Previous theoretical [39-42] and experimental [43] analyses have demonstrated that fluid pressurization contributes to supporting upwards of 90% of the applied stress during contact of cartilage layers. This suggests that fluid pressure could act to shield the solid matrix of cartilage [44]. The pressure presumably stimulates cells to synthesise proteoglycans (PG), the function of which is to resist pressure [33]. In this study the pore pressure results at the cartilage model during the stance phase showed that most of the cartilage volume delimited by the contact area was subject to pore pressure values lower than 0.035MPa, while the remaining cartilage volume can reach maximum pore pressure values of 0.21MPa. This pressure values are in line with the study of Kazemi et al. [45], where the fluid pressurization was analysed in knee joints. In a general way, the agarose construct models presented pore pressure values lower than the ones found in the cartilage model. Most of the

agarose volume presented pore pressure values four times less than the observed at the cartilage model. The increase of compressive strain, as well as of applied frequency has a tendency to increase the volume of the agarose construct subjected to the highest pore pressure values. This pore pressure behaviour is in agreement with the experimental study of Soltz and Ateshian [46], where pressurization takes place with increasing loading frequency. Of the nine loading regimes applied on the agarose models, the loading regime with 20% of compression strain at 3Hz was the one that best approximates the volume fraction by pore pressure range of the cartilage model.

A previous experimental study in cartilage explants showed stimulation of PG synthesis in areas of the tissue with high interstitial fluid velocities [18]. Fluid velocity results in the cartilage model showed that more than 83.3% of cartilage volume during a load cycle had values lower than 0.165μm/s. In the agarose construct model, for all loading regimes analysed only 1-3% of the agarose volume had fluid velocities lower than 0.165μm/s, and more than 65% of the agarose volume presented fluid velocities greater than 1μm/s. The observed fluid velocity differences show the incapacity of direct dynamic compression at physiologic loading regimes to produce a fluid velocity stimulus comparable to native cartilage levels. Due to high fluid velocities developed at the agarose construct, and the fact that these high fluid velocities are associated with high proteoglycan synthesis [17] this may explain the large content of proteoglycan found in agarose constructs subjected to physiologic loading regimes [47-48].

The relationships between the intrinsic mechanical stimuli analysed and some metabolic outcomes described previously highlights the importance of the evaluation of the intrinsic mechanical stimuli of native cartilage, as well as the ability to replicate these on the chondrocyte-seeded constructs, two important key issues in tissue-engineered cartilage. For the maximum principal strain stimulus, the loading regime which better reproduces the cartilage model was the lowest compression strain and frequency regime tested, while for the pore pressure stimulus, the loading regime that best reproduces the volume fraction by pore-pressure range of the cartilage model was the highest compression strain

and frequency regime. Nevertheless, for the fluid velocity stimulus, none of the nine physiological regimes applied to the agarose construct was capable to approximate the volume fraction by fluid velocity range of the cartilage model, suggesting the need of a lower compressive strain and frequency loading regime (<5% and <0.5Hz). These results suggest that the initial direct dynamic compression loading regime needs to be designed differently throughout the culture period in order to better reproduce the mechanical outputs of the native cartilage. Based on our results, an initial loading regime which combines periods of low compressive strain and frequency (5%Hz at 0.5Hz), in order to approach closer maximum principal strain stimulus to the native cartilage, with time periods of high compressive strain and frequency (20% at 3Hz), in order to approach the pore pressure values of the native cartilage model, may be advantageous relatively to a single physiologic loading regime during all the culture period.

As in all numerical studies, our study has some shortcomings, just like the experimental studies and like studies published by others that should be kept in mind while interpreting the results of the present study. The patient-specific knee model was simplified in terms of the applied loads and the structural links. However, the cyclic loading patterns applied to the specimen-specific tibiofemoral cartilage were taken from *in vivo* tibiofemoral cartilage deformation data during the stance phase of gait [20], which ensures a more valid simulated load condition in specimen-specific cartilage. Another simplification is that the agarose models have not taken in account the ECM production during culture time. Being this study a comparative one, the variations caused by the ECM elaboration are expected to induce similar effects with time for all the different loading regimes analysed. Other limitation of this study is related with the dimensions of the agarose construct, which can influence the magnitude and distribution of the intrinsic mechanical stimuli. We have used construct dimensions in the range presented on several experimental studies [5, 8, 11, 49] and compatible with a transplant in human tibiofemoral joint.

5. CONCLUSION

Efficacy assessment on intrinsic mechanical stimulus developed in the articular cartilage and cell-seeded constructs is crucial to increase the competence of tissue-engineering strategies. In this study, intrinsic mechanical stimuli for a physiological spectrum of loading patterns applied on agarose constructs demonstrated a limited capacity to replicate each one of the intrinsic mechanical stimuli developed on specific-patient cartilage. This suggests that direct dynamic compression loading regime, needs to be differently parameterized in terms of applied strain and frequency during the culture period. An initial loading regime which combines time periods of low compressive strain and frequency, in order to approach the maximal principal strain and fluid velocity stimulus of the patient-specific cartilage, with time periods of high compressive strain and frequency, in order to approach the pore pressure values, may be advantageous relatively to a single loading regime throughout the full culture period.

ACKNOWLEDGEMENTS

The authors wish to thank: Program COMPETE funding through the projects POCI-01-0145-FEDER-016574, PTDC/EMS-TEC/3263/2014 and Projecto 3599 – PPCDT e comparticipado pelo Fundo Comunitário Europeu FEDER.

Competing interests: None declared

Funding: Program COMPETE funding through the projects POCI-01-0145-FEDER-016574, PTDC/EMS-TEC/3263/2014 and Projecto 3599 – PPCDT e comparticipado pelo Fundo Comunitário Europeu FEDER.

Ethical approval: Hospital Ethic commission and patients consent with judgement number 055-15.

REFERENCES

1. Schulz, R.M., and A. Bader. (2007). Cartilage tissue engineering and bioreactor systems for the cultivation and stimulation of chondrocytes. Eur Biophys J. 36, 539-568.

2. Huang AH, Farrell MJ, Mauck RL. (2010). Mechanics and mechanobiology of mesenchymal stem cell-based engineered cartilage. J Biomech. 43,128–136.

3. Zhang L, Hu J, Athanasiou KA. (2009). The role of tissue engineering in articular cartilage repair and regeneration. Crit Rev Biomed Eng. 37, 1–57.

4. Casanova R, Moukoko D, Pithioux M, Pailler-Mattéi C, Zahouani H, Chabrand P. (2010). Temporal evolution of skeletal regenerated tissue: what can mechanical investigation add to biological? Medical & Biological Engineering & Computing. 48, 811-819.

5. Bian L., Fong J.V., Lima E.G., Stoker A.M., Ateshian G.A., Cook J.L., Hung C.T., (2010). Dynamic mechanical loading enhances functional properties of tissue-engineered cartilage using mature canine chondrocytes. Tissue Eng Part A 16, 1781–1790.

6. Bader DL, Knight MM. (2008). Biomechanical analysis of structural deformation in living cells. Medical & Biological Engineering & Computing. 46, 951-963.

7. Kock LM, Schulz RM, van Donkelaar CC, Thummler CB, Bader A, Ito K (2009). RGD-dependent integrins are mechanotransducers in dynamically compressed tissue-engineered cartilage constructs. J Biomech 42:2177–2182.

8. Mauck RL, Seyhan SL, Ateshian GA, Hung CT (2002) Influence of seeding density and dynamic deformational loading on the developing structure/function relationships of chondrocyte seeded agarose hydrogels. Ann Biomed Eng 30:1046–1056.

9. Bhattacharjee M, Coburn J, Centola M, Murab S, Barbero A, Kaplan DL, Martin I, Ghosh S. (2015). Tissue engineering strategies to study cartilage development, degeneration and regeneration. Advanced Drug Delivery Reviews, 84, 107-122.

10. Kock L., van Donkelaar C.C., Ito K. (2012). Tissue engineering of functional articular cartilage: the current status. Cell Tissue Res 347:613–627.

11. Tsuang YH, Lin YS, Chen LT, (2008); Effect of dynamic compression on in vitro chondrocyte metabolism. Int J Artif Organs 31: 439–449.

12. Park S, Hung CT, Ateshian GA. (2004). Mechanical response of bovine articular cartilage under dynamic unconfined compression loading at physiological stress levels. Osteoarthritis Cartilage. 12(1):65-73.

13. Lee DA, Noguchi T, Frean SP, Lees P, Bader DL. (2000). The influence of mechanical loading on isolated chondrocytes seeded in agarose constructs. Biorheology. 37(1-2):149-61.

14. Lee DA, Bader DL. (1997). Compressive strains at physiological frequencies influence the metabolism of chondrocytes seeded in agarose. J Orthop Res. 15(2):181-8.

15. Jeon J.E., Schrobback K., Hutmacher D.W., Klein T.J. (2012) Dynamic compression improves biosynthesis of human zonal chondrocytes from osteoarthritis patients. Osteoarthritis and Cartilage 20, 906-915.

16. Butler DL, Goldstein SA, Guldberg RE, Guo XE, Kamm R, Laurencin CT, McIntire LV, Mow VC, Nerem RM, Sah RL, Soslowsky LJ, Spilker RL, Tranquillo RT., (2009). The impact of biomechanics in tissue engineering and regenerative medicine. Tissue Eng Part B Rev. 15(4), 477-84.

17. Hung C.T., Mauck R.L., Wang C.C., Lima E.G., Ateshian G.A. (2004). A Paradigm for Functional Tissue Engineering of Articular Cartilage via Applied Physiologic Deformational Loading. Annals of Biomedical Engineering, 32; 35–49.

18. Buschmann, M. D., Y.-J. Kim, M. Wong, E. Frank, E. B. Hunziker, and A. J. Grodzinsky., (1999). Stimulation of aggrecan synthesis in cartilage explants by cyclic loading is localized to regions of high interstitial fluid flow. Arch. Biochem. Biophys. 366; 1–7.

19. Tasci A., Ferguson S.J., Buchler P. (2011). Numerical assessment on the effective mechanical stimuli for matrix-associated metabolism in chondrocyte-seeded constructs. J Tissue Eng Regen Med; 5; 210–219.

20. Liu F., Kozanek M., Hosseini A., Van de Velde S.K. Gill TJ, Rubash HE, Li G, (2010). In vivo tibiofemoral cartilage deformation during the stance phase of gait. J Biomech, 43, 4, 658-665.

21. Peng L, Bai J., Zeng X, Zhou Y, (2006). Comparison of isotropic and orthotropic material property assignments on femoral finite element models under two loading conditions. Medical Engineering & Physics 28, 3, 227–233.

22. Keller TS. (1994). Predicting the compressive mechanical behavior of bone. J Biomech. 27(9); 1159–1168.

23. Boschetti F, Pennati G, Gervaso F, Peretti GM, Dubini G., (2004). Biomechanical properties of human articular cartilage under compressive loads. Biorheology. 41(3-4); 159-66.

24. Holmes, M. H., and Mow, V. C.(1990). The nonlinear characteristics of soft gels and hydrated connective tissues in ultrafiltration. Journal of Biomech 23(11), 1145-1156.

25. Gu WY, Yao H, Huang CY, Cheung HS. (2003). New insight into deformation-dependent hydraulic permeability of gels and cartilage, and dynamic behavior of agarose gels in confined compression. J Biomech. 36:593–598.

26. van der Voet A. (1997). A comparison of finite element codes for the solution of biphasic poroelastic problems. Proc Inst Mech Eng H. 211, 209–211.

27. Wilson W, van Donkelaar CC, van Rietbergen B, Huiskes R. (2005). A fibril-reinforced poroviscoelastic swelling model for articular cartilage. J. Biomech. 38, 1195–1204.

28. Bandeiras C., Completo A. (2013). Comparison between constitutive models for the solid phase of biphasic agarose/chondrocytes constructs for knee cartilage engineering. Computer Methods in Biomechanics and Biomedical Engineering, 16, 262-263.

29 Bandeiras C., Completo A., Ramos A., (2014). Compression, shear and bending on tissue-engineered cartilage: a numerical study. Computer Methods in Biomechanics and Biomedical Engineering, 17,-3.

30.Bandeiras C., Completo A., (2015). Comparison of mechanical parameters between tissue engineered and native cartilage: a numerical study. Computer Methods in Biomechanics and Biomedical Engineering, 18, 1876-7

31 Bandeiras, C., Completo, A., Ramos, A., Rufino, T., Ribeiro, M., Ferreira, J.P., Mendes, A., (2015). "Tissue engineered cartilage in unconfined compression: biomechanical analysis". Materials Today: Proceedings, 2:1, 355-364.

32 Bandeiras C Completo, A., Ramos, A. (2015). Influence of the scaffold geometry on the spatial and temporal evolution of the mechanical proprieties of tissue engineered cartilage: Insights from a mathematical model. Biomechanics and Modeling in Mechanobiology, 14, 1057-1070

33 Khoshgoftar M, van Donkelaar CC, Ito K. (2011). Mechanical stimulation to stimulate formation of a physiological collagen architecture in tissue-engineered cartilage: a numerical study. Comput Methods Biomech Biomed Engin. 14(2), 135-144.

34 Muralidharan P. (2006). Finite deformation biphasic material characterization and modeling of agarose gel of functional tissue engineering applications [master's thesis]. University of Cincinnatti.

35 Nakatsuji N, Johnson KE. (1984). Experimental manipulation of a contact guidance system in amphibian gastrulation by mechanical tension. Nature. 307(5950):453–455.

36 Fukubayashi T, Kurosawa H. (1980). The contact area and pressure distribution pattern of the knee. A study of normal and osteoarthritic knee joints. Acta Orthop Stand 1980; 51: 871-879.

37 Marzo, J.M., Gurske-DePerio, J., (2009). Effects of medial meniscus posterior horn avulsion and repair on tibiofemoral contact area and peak contact pressure with clinical implications. Am J Sports Med 37(1); 124–129.

38 Driessen NJB, Wilson W, Bouten CVC, Baaijens FPT. (2004). A computational model for collagen fibre remodelling in the arterial wall. J Theoret Biol. 226:53–64.

39 Ateshian, G.A., Wang, H., Lai, W.M. (1998). The role of interstitial fluid pressurization and surface porosities on the boundary friction of articular cartilage. Journal of Tribology 120, 241-248.

40 Julkunen P., Wilson W., Jurvelin JS., Korhonen RK. (2009). Composition of the pericellular matrix modulates the deformation behaviour of chondrocytes in articular cartilage under static loading. Medical & Biological Engineering & Computing. 47, 1281-1290.

41 Kelkar, R., and G. A. Ateshian. (1999). Contact creep of biphasic cartilage layers: Identical layers. J. Appl. Mech. 66; 137–145.

42 Li LP., Cheung JTM., Herzog W. (2009). Three-dimensional fibril-reinforced finite element model of articular cartilage. Medical & Biological Engineering & Computing. 47, 607-615.

43 Oloyede, A., and N. D. Broom. (1991).Is classical consolidation theory applicable to articular cartilage deformation? Clin. Biomech. 6; 206–212.

44 Maroudas, A., and C. Bannon. (1981). Measurement of swelling pressure in cartilage and comparison with the osmotic pressure of constituent proteoglycans. Biorheology. 18:619–632.

45 Kazemi M, Li LP, Savard P, Buschmann MD. (2011). Creep behavior of the intact and meniscectomy knee joints. J Mech Behav Biomed Mater. 4(7), 1351-8.

46 Soltz, M. A., and G. A. Ateshian. (1998). Experimental verification and theoretical prediction of cartilage interstitial fluid pressurization at an impermeable contact interface in confined compression. J. Biomech. 31, 927–934.

47 Hu JC, Athanasiou KA. (2006). A self-assembling process in articular cartilage tissue engineering. Tissue Eng. 12: 969–979.

48 Asanbaeva A., Masuda K., Thonar E.J.M., Klisch S.M., Sah R.L. (2007). Mechanisms of cartilage growth: modulation of balance between proteoglycan and collagen in vitro using chondroitinase ABC. Arthritis Rheum 56, 188–198.

49 Vaughan NM., Grainger J., Bader DL., Knight MM. (2010). The potential of pulsed low intensity ultrasound to stimulate chondrocytes matrix synthesis in agarose and monolayer cultures. Medical & Biological Engineering & Computing. 48, 1215-1222.

TABLES

Table 1 - Peak cartilage deformation of experimental data (Liu et al. 2010) and tibiofemoral deformation applied at the specimen-specific model at 0%, 30%, 60% and 90% of stance phase.

Stance Phase (%)	Experimenatl data (Liu et al., 2010) Peak cartilage deformation		Specimen-specific tibiofemoral model Maximal deformation	
	Medial	Lateral	Medial	Lateral
0%	8,0%	7,0%	8,9%	8,1%
30%	23,0%	16,0%	23,5%	14,9%
60%	15,5%	10,0%	14,0%	11,5%
90%	20,0%	12,0%	21,5%	12,3%

LIST OF FIGURES

Figures

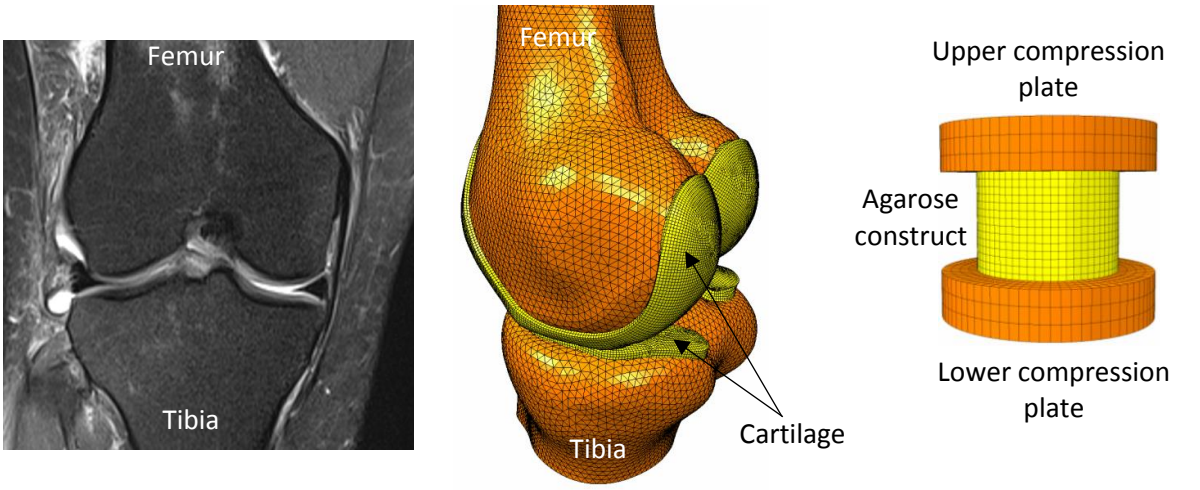

Figure 1

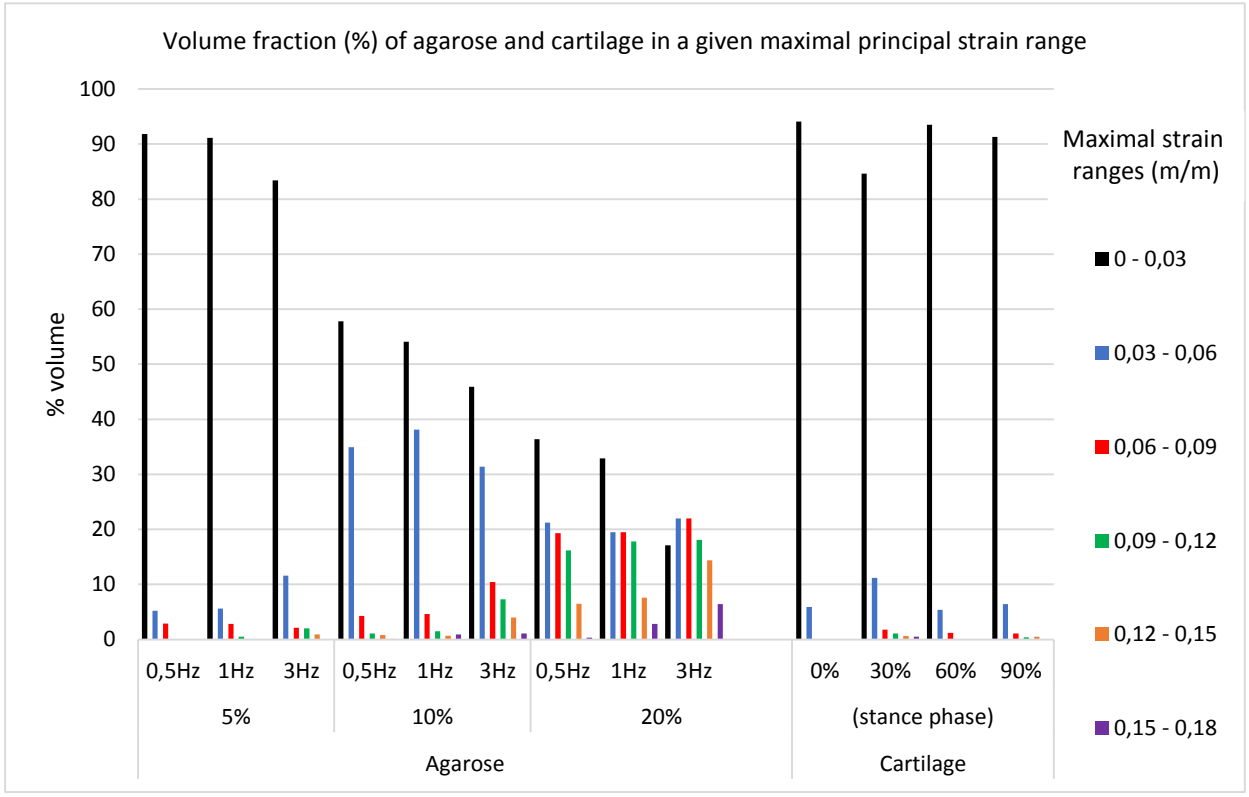

Figure 2

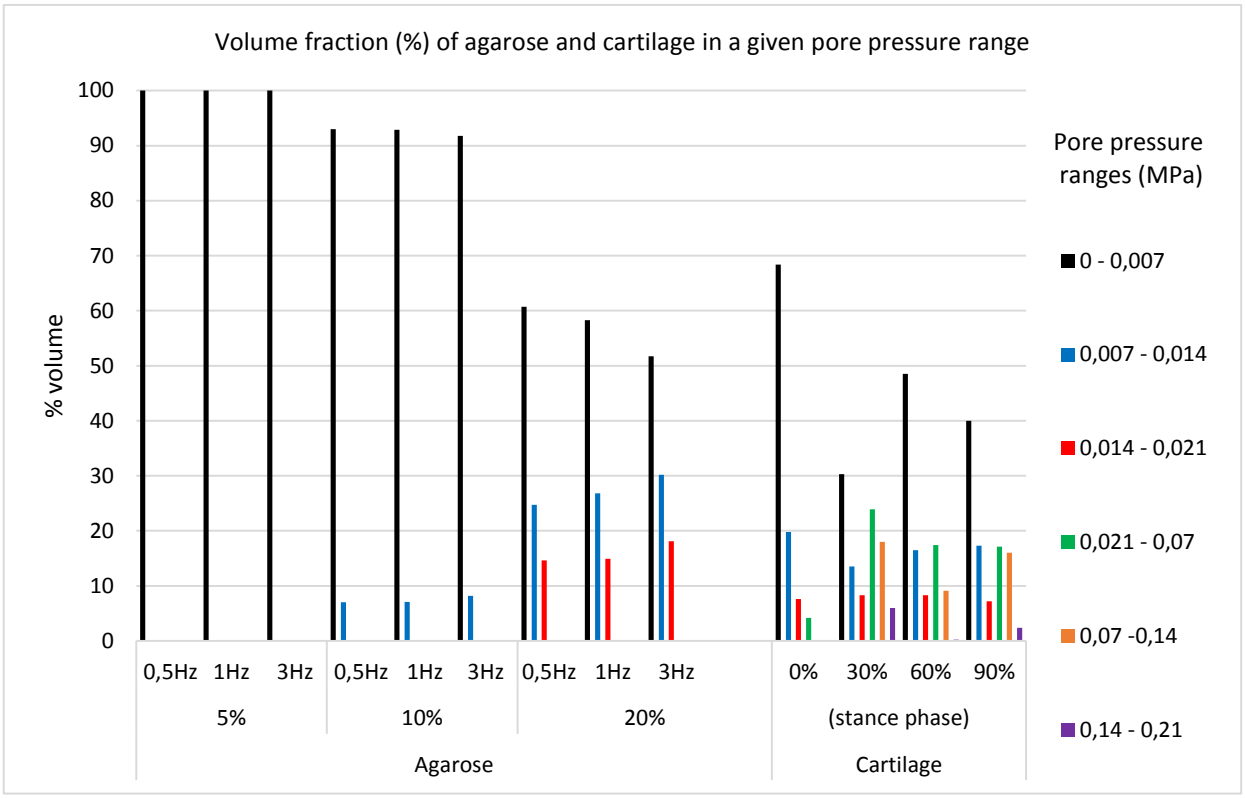

Figure 3

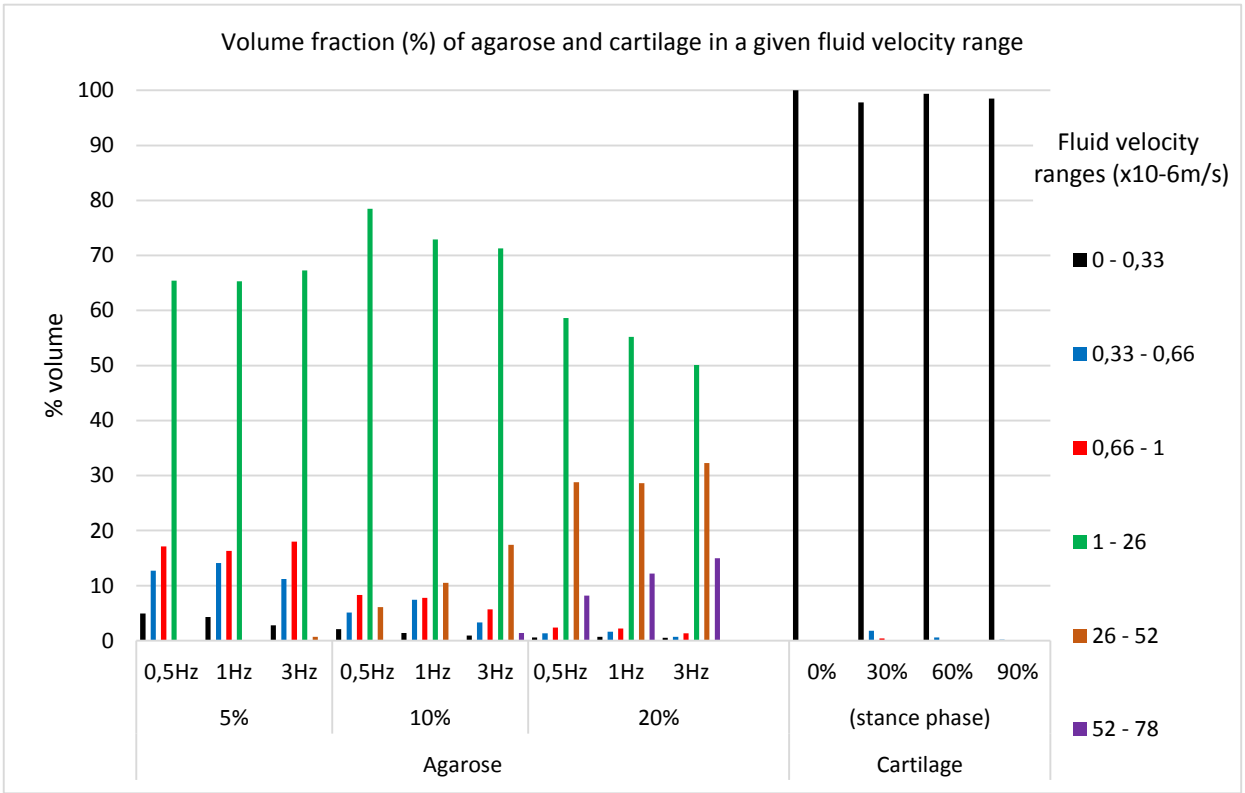

Figure 4